Image Analysis in Modern Ophthalmology: From Acquisition to Computer Assisted Diagnosis and Telemedicine

Andrés G. Marrugo[a], María S. Millán[a], Gabriel Cristóbal[b], Salvador Gabarda[b], Michal Šorel[c], and Filip Šroubek[c]

[a]Department of Optics and Optometry, Universitat Politècnica de Catalunya Violinista Vellsolà 37, 08222 Terrassa, Spain.

[b]Instituto de Óptica, Consejo Superior de Investigaciones Científicas Serrano 121, 28006 Madrid, Spain.

[c] Institute of Information Theory and Automation, Academy of Sciences of the Czech Republic, Pod Vodárenskou věží 4, 18208 Prague 8, Czech Republic.

ABSTRACT

Medical digital imaging has become a key element of modern health care procedures. It provides visual documentation and a permanent record for the patients, and most important the ability to extract information about many diseases. Modern ophthalmology thrives and develops on the advances in digital imaging and computing power. In this work we present an overview of recent image processing techniques proposed by the authors in the area of digital eye fundus photography. Our applications range from retinal image quality assessment to image restoration via blind deconvolution and visualization of structural changes in time between patient visits. All proposed within a framework for improving and assisting the medical practice and the forthcoming scenario of the information chain in telemedicine.

Keywords: Computer-aided diagnosis, medical image, retinal image, telemedicine, ophthalmology.

1. INTRODUCTION

Ophthalmology is no longer a stand-alone branch of medicine conducted exclusively by specialists with the sole purpose of providing medical aid for the visual health of the general population–it is much, much more than that. As it is conceived today, ophthalmology is undisputedly an interdisciplinary field in both research and clinical practice. A field that in the last decade has shown that digital information based systems can be both clinical and cost effective with high levels of patient satisfaction.[1] However, successful deployment is not without great difficulty.

While ophthalmology *per se* involves a great number of sub-specialties and also an ever increasing number of probing techniques, this work focuses on the main ocular fundus imaging modality: color fundus photography. Fundus imaging or fundus photography is basically the process whereby a 2D-representation of the 3D-retinal tissues projected onto the imaging plane is obtained using reflected light.[2] In color fundus photography the image intensities represent the amount of reflected red (R), green (G), and blue (B) wavebands, as determined by the spectral sensitivity of the sensor. Fundus imaging plays a key role in the diagnosis and management of ophthalmologic disorders, such as diabetic retinopathy, glaucoma, and age-related macular degeneration; all of them being the most prevalent causes of blindness in the industrialized world.[2]

In this paper we provide a brief introduction to image analysis in modern ophthalmology that comprises a general view of the field, the presentation of several examples of image analysis techniques, and perspectives on future developments in the field.

Further author information: (Send correspondence to A.G. Marrugo)
A.G.M.: E-mail: andres.marrugo@upc.edu, Telephone: +34 93 739 8678; http://www.goapi.upc.edu/

1.1 A link to the past

The eye fundus has been observed since 1850 with the invention of the ophthalmoscope by the German physician Hermann Von Helmholtz.[3] This was an instrument that enabled the examination of the retina by using a bright light near the eye and shining it into the patient's pupil. However, it was not until the mid 1920s that the Carl Zeiss Company made available the first commercial fundus camera. Many were the limitations in clinical use of fundus photography in the 1930s and 1940s which can be attributed to the difficulty in obtaining good quality images.[3] Significant progress was made in later decades and fundus photography became ubiquitous in the practice of ophthalmology providing a means for recording, storing, and indexing at low cost the images of a patient. This opened many possibilities: specific patients could easily be recorded and catalogued, longitudinal changes could be documented, and later retrieval of images could foster scientific research. Other important imaging modalities appeared only to enhance diagnostic and observational capabilities in ophthalmology such as: fluorescent angiography, modern digital fundus photography, stereo fundus photography, confocal laser opthalmoscopy, and optical coherence tomography. Out of all of these imaging modalities, however, it may be said that fundus photography is the one that provides a more general fundus examination with relatively simple and affordable equipment, and little patient intervention. Interestingly, it has been suggested that information extracted from the eye fundus could be useful in a variety of diseases such as heart disorders, stroke, hypertension, peripheral vascular disease and diabetic retinopathy.[4]

1.2 The new paradigm: computer-aided diagnosis and telemedicine

With the advances of computer technology, various types of computer-aided diagnosis (CAD) systems[5,6] have been developed in recent years. The main idea of CAD is to assist medical staff in interpreting medical images by using dedicated computer systems to provide "second opinions". The final medical decision is made by the physicians. Studies on CAD systems show that it can help to improve diagnostic accuracy, lighten the burden of increasing workload, reduce missed disease detection due to fatigue, overlooked data, and improve inter- and intra-reader variability.[5,7] Meanwhile a number of fundus image CAD systems have also been developed for the diagnosis of various types of ocular diseases such as glaucoma,[8] and diabetic retinopathy.[9,10] These CAD systems have the potential to provide an alternative solution to mass screening programs that need to examine a vast number of fundus images as fast as possible. In a recent work by Sánchez *et al.*,[10] they were able to show that the performance of a CAD system for diabetic retinopathy screening could be comparable with that of human experts. However, while this represents unprecedented performance for CAD systems it does not translate readily to clinical practice. Furthermore, this should not be understood in the sense that CAD systems are to replace specialists, instead they are to ensure that specialists spend more time dealing with the ill by serving the purpose of screening. Nevertheless, further extensive and thorough evaluation is still needed before deployment in clinical practice.

In other regards, CAD systems are also pivotal to the practice of telemedicine. Telemedicine is basically the use of telecommunication and information technologies in order to provide clinical health care at a distance. Traditional examination of the retina requires dilated pupils, a skilled examiner, and a visit to the ophthalmologist, typically in a separate location from the primary care center. Numerous studies in the United States have shown that many diabetes patients fail to seek or receive this important examination on a regular basis.[11] This shortfall has been attributed to a variety of factors but mainly due to socioeconomic and health system barriers. These problems can be overcome by incorporating retinopathy screening into primary care practices, using telemedicine powered by CAD systems for the evaluation of retinal images. The screening process can be simpler and more cost-efficient than sending the patients to the ophthalmologist's office for a live evaluation. A successful and reliable telemedicine retinopathy screening system must be comparable to a live retinal examination in the detection of vision-threatening retinopathy. There are a number of constraints so as to achieve an adequate sensitivity and specificity, and to date there is no general consensus on how to approach them. Meanwhile, a promising strategy rises from the use of license-free web-based software, standard interfaces, and flexible protocols to allow primary care providers to adopt retinopathy screening with minimal effort and resources.[11]

2. PREPROCESSING OF RETINAL IMAGES

The main purpose of preprocessing techniques is to reduce the effect of image variation via normalization of the retinal image against a reference model or data set for subsequent visualization, processing or analysis.

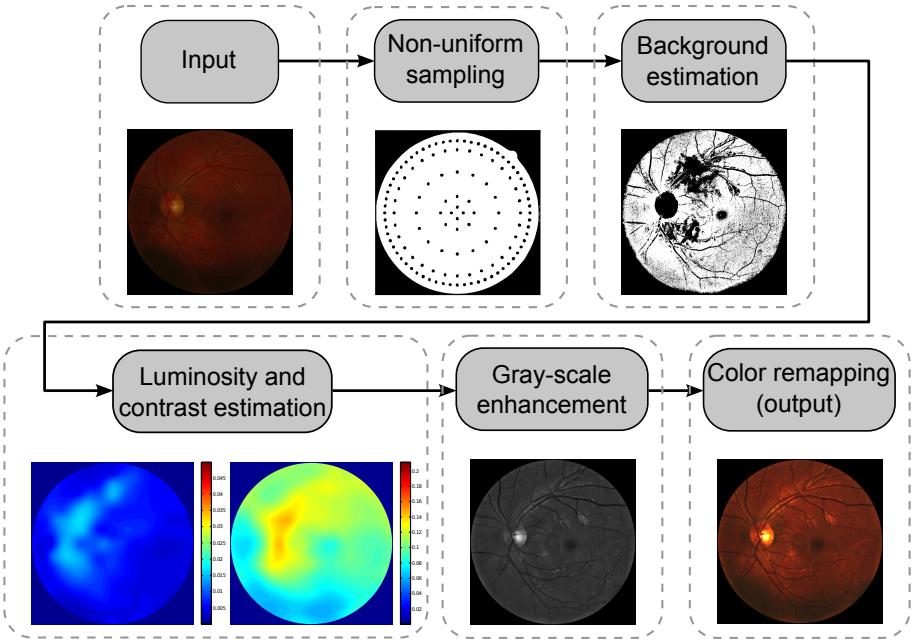

Figure 1. Illumination compensation algorithm

Variations may occur within the same image or between images. The main differences between images are most likely due to differences in cameras, illumination, field of view and retinal pigmentation. Thus, in order to extract meaningful information from an image, it is necessary to compensate for this variability. General preprocessing tasks for both monochromatic and color retinal images may be broadly categorized in terms of the correction for non-uniform illumination, contrast enhancement and color normalization.[12]

Despite controlled conditions, many retinal images suffer from non-uniform illumination. The curved retinal surface and the geometrical configuration of the light source and camera, lead to a poorly illuminated periphery. This problem can be approached in a number of ways. There have been many works on this topic,[12] however they can be loosely classified into single image or multiple image compensation techniques. Several single image techniques have been used to enhance retinal images. Histogram equalization has been shown to be inappropriate for retinal images.[13] A local normalization of each pixel to zero mean and unit variance aims to compensate lighting variation and enhancing local contrast but also introduces artifacts.[13] Histogram matching between the red and green planes has been used as a preprocessing step for vessel segmentation.[14] This improves the contrast of gross dark features like vessels but reduces the contrast of bright objects and tiny dark objects like micro-aneurysms. While most of the aforementioned methods are motivated by automatic analysis, as a preprocessing stage, they are all formulated for a single color plane or for gray-scale images. Color retinal image enhancement is required for human visual inspection or for the application of vector processing techniques.

An example of a single image illumination compensation algorithm is depicted in Fig. 1. This algorithm was described in Ref. 15 and is based on a simple model of degradation proposed by Foracchia *et al.*[16] The main idea is that the image can be enhanced by estimating the background luminosity and contrast distribution in order to compensate for uneven illumination. Therefore, the enhanced image $U(x, y)$ is expressed as:

$$U(x,y) = \frac{I(x,y) - L(x,y)}{C(x,y)} \quad , \tag{1}$$

where I is the original degraded image, C and L are the contrast and luminosity drifts, respectively. C and L can also be understood in terms of gain and offset. They have to be estimated by sampling the original image. This is achieved by using a non-uniform sampling grid as shown in Fig. 1. The sampling is coarse in the central region and dense in the periphery. This is carried out on the green channel of the RGB retinal image because is the channel with highest contrast. The background pixels are estimated by a procedure described in

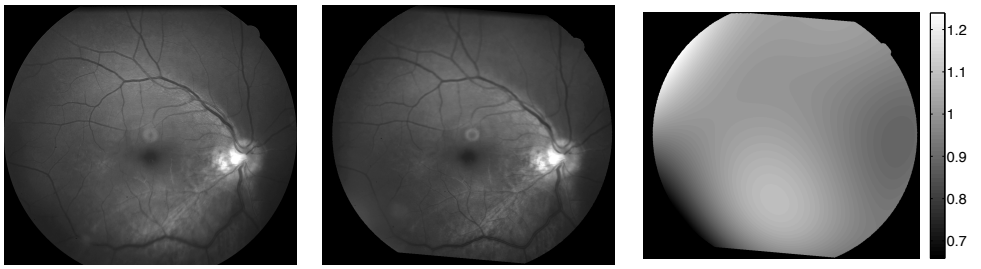

(a) (b) (c)

Figure 2. Illumination compensation for two retinal images (a) and (b). (c) Compensation function k.

Ref. 15. From these pixels the background luminosity and contrast components are computed to produce the image enhancement given by Eq. (1). The final color enhanced retinal image is obtained by performing a color remapping on the gray-scale image that preserves the RGB ratios, however it may introduce color modifications.

Multiple image illumination compensation techniques are mainly motivated by the need for a processing strategy that requires two or more images, e.g. image comparison or change detection,[17] multichannel deconvolution,[18] sequential multispectral imaging,[19] etc. In Ref. 20 we described such a technique for compensating the uneven illumination distribution from two images of the same retina acquired at different moments for further processing. The basic idea is a follows: the illumination distribution can be compensated by adjusting the intensity values on one image to approximately match that of the other while satisfying a predetermined illumination model. Because the illumination of the retina is formed by a slowly varying light field over a smooth surface it can be modeled by a low-order parametric surface, in this case a 4th-order polynomial. The compensation is then formulated via a parametric surface fitting equation

$$\arg\min_{k} \|I_1(x,y) - k(x,y) \cdot I_2(x,y)\| \ , \tag{2}$$

where I_1 and I_2 are the two retinal images, k is the illumination compensation function given by $k(x,y) = \alpha_{15}y^4 + \alpha_{14}y^3x + \cdots + \alpha_2 y + \alpha_1$. Eq. (2) is minimized in the least squares sense to estimate the 15 parameters. In Fig. 2 we show an example of two retinal images and the compensation function $k(x,y)$. The different shades of gray indicate the average contrast and intensity difference between the two original images in Figs. 2(a) and (b).

3. DETECTION OF LONGITUDINAL CHANGES IN RETINAL IMAGES

One of the main concerns of ophthalmologists when they visually compare fundus images of the same retina over time is to identify true structural or morphological changes pertaining to possible pathological damage. In the same inspection they must disregard other changes merely caused by variation of illumination or blur. A correct assessment of a patient's state evolution requires sharp images obtained on a regular time basis. However, this is not always guaranteed and is the main motivation for developing preprocessing techniques as the ones described in the previous section. Image registration is another preprocessing technique necessary for image-based longitudinal change assessment.[12]

In this section we briefly describe a strategy for the identification of areas of structural change in time sequences of retinal images.[20] An initial step in order to identify these changes comes from computing the difference from the two registered images with previous illumination compensation,

$$\Delta I(x,y) = I_1(x,y) - I_2(x,y) \ . \tag{3}$$

An example of a difference image is shown in Fig. 3(c) in absolute value for visualization purposes. The structural changes can now be visualized and detected from the difference image $\Delta I(x,y)$ by taking a statistical significance test, as proposed in Ref. 17. First, structural changes are often associated with a group of pixels, thus the change decision at a given pixel j should be based on a small block of pixels in the neighborhood

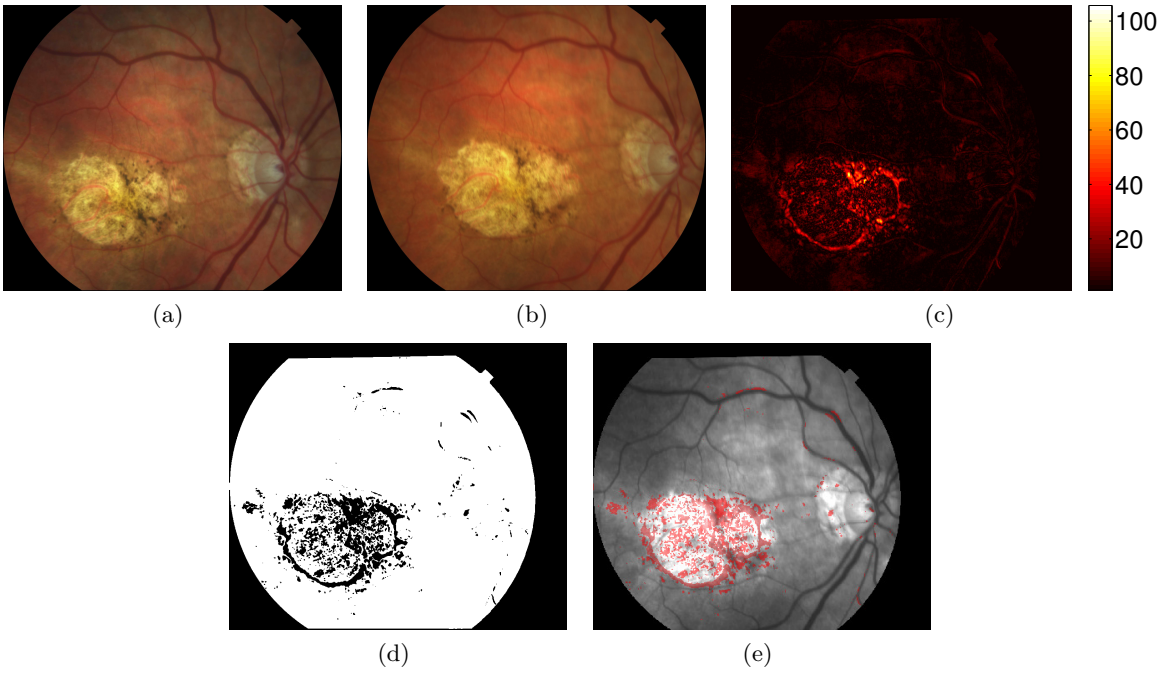

Figure 3. Retinal image change detection: Images (a) I_1 and (b) I_2, (c) Image difference $\Delta I(x, y)$ in absolute value, (d) Image change map, and (d) Image change map in red on top of gray-scale retinal image.

of j denoted as w_j. Second, in the absence of any change, the difference can be assumed to be due to noise alone. Therefore, the decision as to whether or not a change has occurred corresponds to choosing one of two competing hypothesis: the *null hypothesis* $\mathcal{H}_0$ or the *alternative hypothesis* $\mathcal{H}_1$, corresponding to *no-change* and *change* decisions, respectively. Assuming a Gaussian distribution for the difference values, the changes can be identified by comparing the normalized sum square of the differences within the neighborhood w_j to a predetermined threshold τ as described by Aach et al.[21] The test is carried out as below

$$\Omega_j = \frac{1}{\sigma_n^2} \sum_{(x,y)\in w_j} \Delta I(x,y)^2 \underset{\mathcal{H}_0}{\overset{\mathcal{H}_1}{\gtrless}} \tau \ , \tag{4}$$

where σ_n is the noise standard deviation of the difference in the no-change regions. The threshold τ is derived from the fact that Ω_j follows a χ^2 distribution with N degrees of freedom, where N is the number of pixels in the window w_j. It can be obtained for a particular false positive rate α from the χ^2 tables. The image change map resulting from the change detection test with an $\alpha = 0.05$ is shown in Fig 3(d). Notice that the central whitish region (pathological area) is the main cause of structural changes. To better understand this result, in Fig. 3(e) we show one of the retinal images in gray-scale where the pixels related to structural changes are highlighted in red. For further details the reader is referred to Ref. 20.

4. RETINAL IMAGE RESTORATION

In addition to uneven illumination fundus images often suffer from blurring. This hinders diagnosis and the evolution assessment of a disease. In this section we describe a method for fundus image deblurring by means of multichannel blind deconvolution. It consists of a series of preprocessing steps to adjust the images so they comply with the considered degradation model, followed by the estimation of the point spread function, and image deconvolution.

Blind deconvolution consists in the recovery of the original scene from a single or set of blurred images in the presence of a poorly determined or unknown point spread function (PSF).[22] Here we consider multichannel blind deconvolution because it is better posed, as opposed to single-channel, and the PSF is estimated directly

from the degraded images. The restoration strategy is given in Ref. 20. As a regularization term it includes the total variation of the image, which provides good quality of restoration. To properly restore the images the degradation should be adequately modeled.

We assume two registered input images, I_1 and I_2, both originating from an ideal sharp image U

$$\begin{aligned} I_1 &= U * h_1 + n_1 \\ I_2 &= \left(U k^{-1}\right) * h_2 + n_2 \ , \end{aligned} \tag{5}$$

where $*$ is the standard convolution, h_i are called convolution kernels or PSFs and k is a function accounting for relative local illumination change between images. For pixels where no illumination changes occur $k \approx 1$. The noise n_i is assumed Gaussian additive with zero mean in both images. Despite the fact that we consider the PSFs to vary in time between the two image acquisitions, we assume them to be spatially invariant within each image.

The PSF estimation and image deconvolution algorithm can be viewed as a Bayesian maximum a posteriori estimation of the most probable sharp image and blur kernels. The algorithm is basically the minimization of the functional

$$\arg \min_{U,h_1,h_2} \frac{1}{2}||U * h_1 - I_1||^2 + \frac{1}{2}||U * h_2 - kI_2||^2 + \lambda_u \int |\nabla U| + \lambda_h ||I_1 * h_2 - kI_2 * h_1||^2, \tag{6}$$
$$h_1, h_2 \geq 0 \ ,$$

with respect to the latent image U and blur kernels h_1 and h_2. The first and second terms measure the difference between the input blurred images and the searched image U blurred by kernels h_1 and h_2. The size of this difference is measured by L_2 norm $||.||$ and should be small for the correct solution. Ideally, it should correspond to the noise variance in the given image. Function k compensates for uneven illumination. The two remaining terms are regularization terms with positive weighting constants λ_u and λ_h. The third term is the total variation of U. It improves stability of the minimization and from the statistical viewpoint incorporates prior knowledge about the solution. The last term is a condition linking the PSFs of both images, which also improves the numerical stability of the minimization. For this procedure we set $\lambda_u = 1000$ and $\lambda_h = 10$. The functional is alternately minimized in the subspaces corresponding to the image and the PSFs. The minimization in the PSF subspace is equivalent to the solution of a system of linear equations in the least squares sense with the non-negativity constraint. In the same minimization procedure both the PSFs and the restored image are estimated. If I_1 and I_2 were acquired in a lapse of time, it would be necessary to introduce the structural change detection strategy (Section 3) in both the model of Eq. (5) and the functional given by Eq. (6) (Ref. 20).

An example of a restored retinal image is shown in Fig. 4. In this example the PSF was estimated by Eq. (6), but we have performed deconvolution (restoration) with a single image and with both images to demonstrate the advantages of using multiple images in the restoration as well. From the profile of the original image not much detail can be properly resolved. In contrast there is a noticeable enhancement in both restored images in such a way that much more details are properly resolved. The multichannel deconvolution overcomes the limitations of single-channel deconvolution due to information redundancy. The improvement in resolution is evidenced by gain in contrast and steeper slopes. Notice the small c-shaped blood vessel within the optic disc, and how they are much sharper and properly resolved in the multichannel restoration in Fig. 4 in comparison with the single-channel restoration and the original images. For a detailed examination of this topic see Refs. 18, 20.

5. RETINAL IMAGE QUALITY ASSESSMENT

Image quality evaluation is a limiting factor for automated retinopathy detection.[2] The imaging procedure is typically carried out in two separate stages: image acquisition and diagnostic interpretation. Image quality is subjectively evaluated by the person capturing the images and they can sometimes mistakenly accept a low quality image. Accurate image quality assessment algorithms can allow operators to avoid poor images. Furthermore, a quality metric would permit the automatic submission of only the best images if many were available.

In this section we provide a short description of the work contained in Ref. 23, where we studied the performance of several state-of-the-art no-reference image quality metrics for retinal imaging. Two examples are

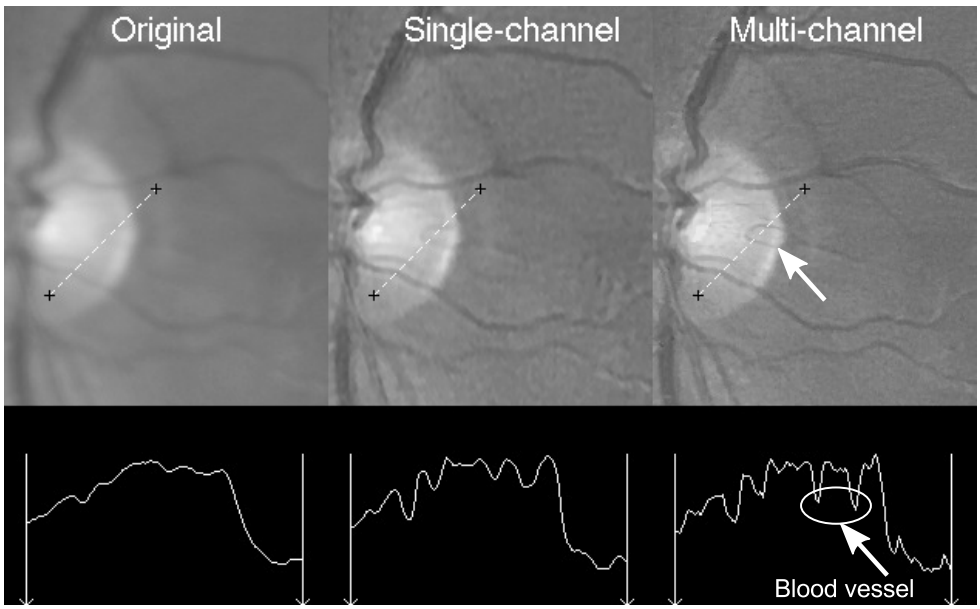

Figure 4. (Top, from left to right) Detail from the original degraded retinal image, the restored version using single-channel deconvolution, and multi-channel deconvolution. (Bottom) Intensity profiles corresponding to the dashed segment. Note how the profiles depict the level of detail in each image.

their application for image quality sorting or image sharpness assessment for focusing. In fact, most no-reference quality assessment methods were initially proposed in the context of focusing applications.[24] The most interesting finding relates to the importance of directional properties with image quality. In other words, the measure of anisotropy as a quality metric. This concept of anisotropy was proposed by two co-authors of this paper (Gabarda and Cristóbal) in Ref. 25 and it represents an important step forward in the area of no-reference quality metrics.

The considered image quality metrics are the following. The first metric Q_1 was proposed by Gabarda and Cristóbal[25] and is based on measuring the variance of the expected entropy of a given image upon a set of predefined directions. The entropy is computed on a local basis using the generalized Rényi entropy and the normalized pseudo-Wigner distribution as an approximation for the probability density function. The authors were able to show that this measure provides a good estimate for the assessment of fidelity and quality in natural images, because their degradations may be seen as a decrease in their directional properties. The second metric Q_2 was proposed by Zhu and Milanfar[26] and it seeks to provide a quantitative measure of –what they call– "true image content". It is correlated with the noise level, sharpness, and intensity contrast manifested in visually salient geometric features such as edges. Q_2 is based upon singular value decomposition of local image gradient matrix. Its value generally drops if the variance of noise rises, and/or if the image content becomes blurry. To avoid regions without edges this algorithm divides the image into small patches and only processes anisotropic ones (non-homogeneous), thus local information is embedded into the final result. The third metric Q_3 was proposed by Ferzli and Karam.[24] It is a sharpness metric designed to be able to predict the relative amount of blurriness in images regardless of their content. Q_3 is conceived on the notion that the human visual system is able to mask blurriness around an edge up to a certain threshold, called the"just noticeable blur" (JNB). It is an edge-based sharpness metric based on a human visual system model that makes use of probability summation over space. JNB can be defined as the minimum amount of perceived blurriness given a contrast higher than the "Just Noticeable Difference". Finally, for the sake of completeness we include the image variance as metric Q_4. This measure has been proven to be monotonic and has a straight-forward relation with image quality for autoregulative illumination intensity algorithms.[27]

In Figs. 5(a)-(b) we show an example of a sharp retinal image and a close-up region for depicting the details of the image. The idea behind this experiment is to determine which quality metric describes better the decreasing image quality. The sharp image was artificially blurred with a 15×15 Gaussian kernel with a varying standard

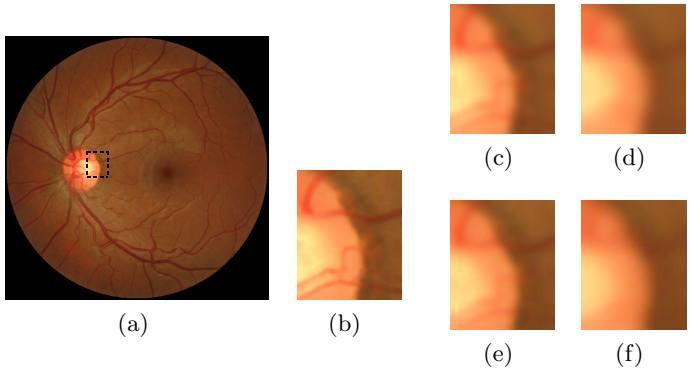

Figure 5. (a) Original sharp retinal image and (b) detail. (c)-(d) details from artificially blurred images with $\sigma = 1.5$ and $\sigma = 3$, respectively. (e)-(f) detail from images with different degrees of focus 3 and 6, respectively (See Fig. 6).

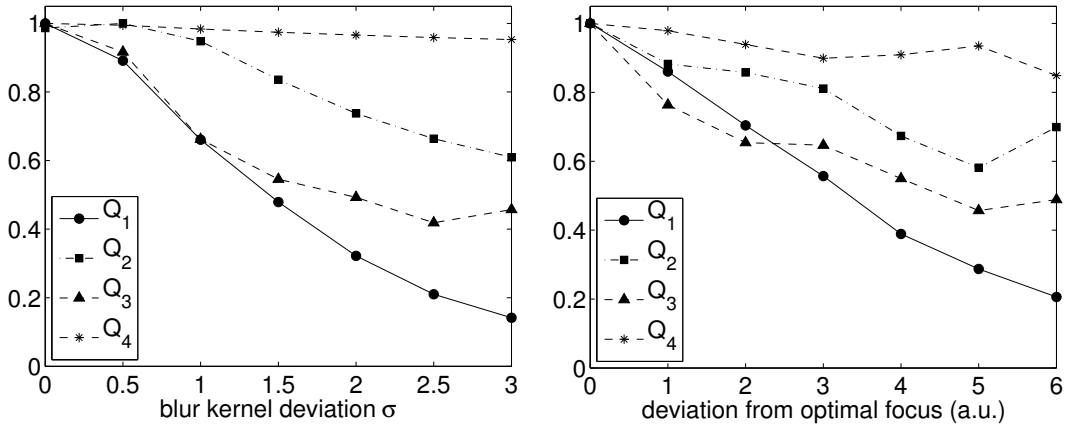

Figure 6. No-reference metrics for assessing image sharpness in relative value. (a) Fundus image artificially blurred with a 15×15 gaussian kernel with varying σ. (b) Fundus images corresponding to the same eye in (a) but with different degrees of fine focus acquired with the retinal camera.

deviation σ. Figs. 5(c)-(d) show the close-up region for the blurred images with $\sigma = 1.5$ and $\sigma = 3$, respectively. The increase in blurriness hinders the resolution of fine structures, hence the medical use is affected as well. In Figs. 5(e)-(f) we show the experimental close-up regions from degraded out of focus images acquired from the same eye fundus.

In Fig. 6(a) we show the resulting quality metrics for the artificial blurring. The figure clearly reveals the overall monotonic nature of all metrics, however Q_1 is the only metric that rapidly decreases with respect to increase in blurriness. The results from the experimental images are shown in Fig. 6(b). Notice how Q_1 also behaves in a consistent way with respect to the deviation from optimal focus. The other metrics seem to be reliable for a considerable amount of blurriness. One possible explanation for the discrepancy between the artificial and real blur for the metrics Q_{2-4} is that the overall illumination distribution cannot be exactly the same, moreover it is also non-uniform. If the metric is not conceived for variations in illumination –even if they were small– it is prone to produce an unreliable result, whereas in Q_1 the intensity normalization provides a certain level of robustness to this type of variation.

In Ref. 23 these experiments led us to conclude that, even though all metrics proved to decrease with the increase in blurriness, strict monotonic decrease was only appreciable for Q_1. This lends strong support for the design of image sharpness metrics based on a directional measure of image content.

6. CONCLUSIONS AND PERSPECTIVES

As we have seen the application of digital image processing techniques for medical image analysis, in this case retinal images, is not only extremely beneficial but can also prove to be effective and cost-efficient for disease management, diagnosis, screening, etc. The increasing need for early detection and screening, along with the ever increasing costs of health care, are likely to be the driving force for the rapid adoption and translation of research findings into clinical practice. The direction of progress, in the short and mid term in this field, is generally conceived within two scenarios: 1) when the amount of data to be analyzed by the medical specialist is excessively large and 2) when the analysis is complex and requires quantification, as opposed to the more qualitative nature of the human expert.

ACKNOWLEDGMENT

This research has been partly funded by the Spanish Ministerio de Ciencia e Innovación y Fondos FEDER (project DPI2009-08879) and projects TEC2010-09834-E and TEC2010-20307. Financial support was also provided by the Czech Ministry of Education under the project 1M0572 (Research Center DAR). The first author also thanks the Spanish Ministerio de Educación for an FPU doctoral scholarship.

REFERENCES

[1] de Mul, M., de Bont, A., and Berg, M., "IT-supported skill-mix change and standardisation in integrated eye-care: lessons from two screening projects in The Netherlands," *International journal of integrated care* **7**(2) (2007).

[2] Abramoff, M. D., Garvin, M., and Sonka, M., "Retinal imaging and image analysis," *IEEE Rev Biomed Eng* **3**, 169–208 (2010).

[3] Saine, P. and Tyler, M., [*Ophthalmic photography: retinal photography, angiography, and electronic imaging*], Butterworth-Heinemann, 2nd ed. (2004).

[4] Bernardes, R., Serranho, P., and Lobo, C., "Digital ocular fundus imaging: A review," *Ophthalmologica* **226**, 161–181 (2011).

[5] Fujita, H., Uchiyama, Y., Nakagawa, T., Fukuoka, D., Hatanaka, Y., Hara, T., Lee, G., Hayashi, Y., Ikedo, Y., Gao, X., and Zhou, X., "Computer-aided diagnosis: The emerging of three CAD systems induced by Japanese health care needs," *Computer Methods and Programs in Biomedicine* **92**(3), 238–248 (2008).

[6] Doi, K., "Computer-aided diagnosis in medical imaging: historical review, current status and future potential," *Comput Med Imag Grap* **31**(4-5), 198–211 (2007).

[7] Lu, S., Liu, J., Lim, J., Zhang, Z., and Meng, T., "Automatic fundus image classification for computer-aided diagonsis.," *31st Annual Int. Conf. of the IEEE EMBS* (2009).

[8] Muramatsu, C., Hayashi, Y., Sawada, A., Hatanaka, Y., Hara, T., Yamamoto, T., and Fujita, H., "Detection of retinal nerve fiber layer defects on retinal fundus images for early diagnosis of glaucoma," *J. Biomed. Opt.* **15**(1), 016021 (2010).

[9] Hatanaka, Y., Nakagawa, T., Hayashi, Y., Mizukusa, Y., Fujita, A., Kakogawa, M., Kawase, K., Hara, T., and Fujita, H., "CAD scheme for detection of hemorrhages and exudates in ocular fundus images," *Medical Imaging 2007: Computer-Aided Diagnosis* **6514**(1), 65142M–8 (2007).

[10] Sánchez, C. I., Niemeijer, M., Dumitrescu, A. V., Suttorp-Schulten, M. S. A., Abramoff, M. D., and van Ginneken, B., "Evaluation of a computer-aided diagnosis system for diabetic retinopathy screening on public data," *Investigative Ophthalmology & Visual Science* **52**(7), 4866–4871 (2011).

[11] Cuadros, J. and Bresnick, G., "EyePACS: an adaptable telemedicine system for diabetic retinopathy screening," *Journal of diabetes science and technology* **3**(3), 509–516 (2009).

[12] Winder, R., Morrow, P., McRitchie, I., Bailie, J., and Hart, P., "Algorithms for digital image processing in diabetic retinopathy," *Comput Med Imag Grap* **33**(8), 608–622 (2009).

[13] Feng, P., Pan, Y., Wei, B., Jin, W., and Mi, D., "Enhancing retinal image by the contourlet transform," *Pattern Recognition Letters* **28**(4), 516 – 522 (2007).

[14] Salem, N. and Nandi, A., "Novel and adaptive contribution of the red channel in pre-processing of colour fundus images," *Journal of the Franklin Institute* **344**(3-4), 243–256 (2007).

[15] Marrugo, A. G. and Millán, M. S., "Retinal image analysis: preprocessing and feature extraction," *Journal of Physics: Conf Series* **274**(1), 012039 (2011).

[16] Foracchia, M., Grisan, E., and Ruggeri, A., "Luminosity and contrast normalization in retinal images," *Med Image Anal* **9**(3), 179–190 (2005).

[17] Narasimha-Iyer, H., Can, A., Roysam, B., Stewart, C., Tanenbaum, H., Majerovics, A., and Singh, H., "Robust detection and classification of longitudinal changes in color retinal fundus images for monitoring diabetic retinopathy," *IEEE Trans Biomed Eng* **53**(6), 1084–1098 (2006).

[18] Marrugo, A. G., Sroubek, F., Sorel, M., and Millán, M. S., "Multichannel blind deconvolution in eye fundus imaging," in [*ISABEL '11-Proceedings of the 4th International Symposium on Applied Sciences in Biomedical and Communication Technologies*], 7:1–7:5, New York, NY, USA (2011).

[19] Everdell, N., Styles, I., Calcagni, A., Gibson, J., Hebden, J., and Claridge, E., "Multispectral imaging of the ocular fundus using light emitting diode illumination," *Review of Scientific Instruments* **81**(9), 093706–093709 (2010).

[20] Marrugo, A. G., Sroubek, F., Sorel, M., and Millán, M. S., "Retinal image restoration by means of blind deconvolution," *J. Biomed. Opt.* **16**(11), 116016 (2011).

[21] Aach, T. and Kaup, A., "Bayesian algorithms for change detection in image sequences using markov random fields," *Signal Processing: Image Communication* **7**(2), 147–160 (1995).

[22] Levin, A., Weiss, Y., Durand, F., and Freeman, W., "Understanding Blind Deconvolution Algorithms," *IEEE Trans. on Pattern Analysis and Machine Intelligence* **33**(12), 2354–2367 (2011).

[23] Marrugo, A. G., Millán, M. S., Cristóbal, G., Gabarda, S., and Abril, H. C., "No-reference quality metrics for eye fundus imaging," *CAIP 2011, Lecture Notes in Computer Science* **6854**, 486–493 (2011).

[24] Ferzli, R. and Karam, L. J., "A no-reference objective image sharpness metric based on the notion of just noticeable blur (JNB)," *IEEE Trans Image Process* **18**(4), 717–28 (2009).

[25] Gabarda, S. and Cristóbal, G., "Blind image quality assessment through anisotropy," *J. Opt. Soc. Am. A* **24**(12), B42–51 (2007).

[26] Zhu, X. and Milanfar, P., "Automatic parameter selection for denoising algorithms using a no-reference measure of image content," *IEEE Trans Image Process* **19**(12), 3116–3132 (2010).

[27] Qu, Y., Pu, Z., Zhao, H., and Zhao, Y., "Comparison of different quality assessment functions in autoregulative illumination intensity algorithms," *Optical Engineering* **45**, 117201 (2006).